Materials Chemistry and Physics 332 (2025) 130143

Contents lists available at ScienceDirect

Materials Chemistry and Physics

journal homepage: www.elsevier.com/locate/matchemphys

Assessing the heat storage potential of zeolitic imidazolate frameworks (ZIFs) using water and ethanol as working fluids

Ciara Byrne [a,b,*], Matjaž Mazaj [a], Nataša Zabukovec Logar [a,b]

[a] National Institute of Chemistry, Hajdrihova 19, SI-1000, Ljubljana, Slovenia
[b] University of Nova Gorica, Vipavska cesta, SI-5000, Nova Gorica, Slovenia

HIGHLIGHTS

- A systematic study on the structural properties for 7 ZIFs and the impact on their heat storage potential.
- The hydrophilicity of the functional groups plays a more significant role in the H_2O uptake compared to the uptake of EtOH.
- ZIF-90 had the highest desorption enthalpy when water is the working fluid, however ZIF-93 is significantly more stable.
- ZIF-93 has the greatest heat storage potential out of the seven ZIFs studied when examining both working fluids.

GRAPHICAL ABSTRACT

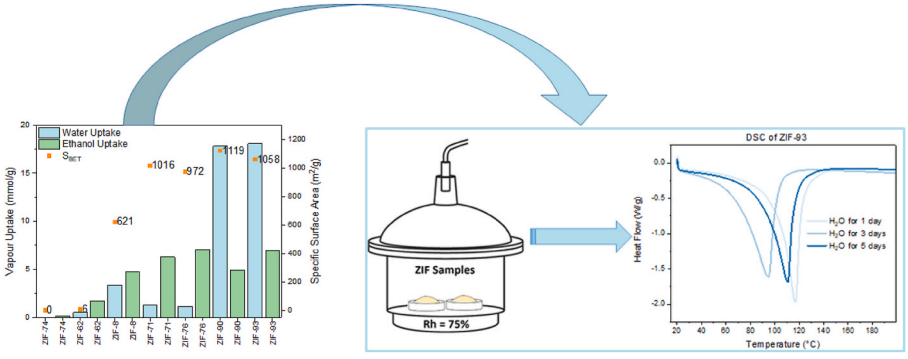

ARTICLE INFO

Keywords:
ZIFs
Sorption studies
Ethanol uptake
Water uptake
Heat storage
Desorption enthalpy

ABSTRACT

Zeolitic imidazolate frameworks (ZIFs) are comprised of transition metal cations such as Zn(II) and imidazolate-based ligands. Due to their inherent properties, including large surface areas, well-defined and stable porous structure, ZIFs hold significant promise for adsorption applications. Sorption-based heat storage and transformation with porous materials and water as working fluid has been recently recognized as one of the most promising approaches to address more efficient use of energy. In this study, we examined seven different ZIFs (ZIF-8, ZIF-62, ZIF-71, ZIF-74, ZIF-76, ZIF-90 and ZIF-93) and their heat storage potential using water and ethanol as working fluids. It has been demonstrated that storage performance is governed by several factors, including pore dimensions, type and distribution of functional groups on imidazolate ligands, chemical stability of the framework as well as the type of the working fluid. Ethanol sorption data demonstrates inflection points in sorption isotherms at lower relative pressures, enhancement of uptakes for ZIFs with hydrophobic properties, but lower desorption enthalpies if compared to water sorption. We found that ZIF-93 was the most promising material for both working fluids.

* Corresponding author. National Institute of Chemistry, Hajdrihova 19, SI-1000, Ljubljana, Slovenia.
E-mail address: ciara.byrne@ki.si (C. Byrne).

https://doi.org/10.1016/j.matchemphys.2024.130143
Received 13 August 2024; Received in revised form 12 November 2024; Accepted 13 November 2024
Available online 15 November 2024

Table 1
Pore entrance size, the pore/cage capacity and topology for the ZIFs examined.

ZIF	d_a^g [Å]	d_p^h [Å]	Topology	Ref.
ZIF-8	3.5	11.6	SOD	[24,25]
ZIF-62	1.4	1.3	CAG	[24,26]
ZIF-71	4.2	16.5	RHO	[24,26]
ZIF-74	1.2	2.6	GIS	[8,24]
ZIF-76	5.4	11.6	LTA	[27]
ZIF-90	3.5	11.2	SOD	[24,28]
ZIF-93	3.6	17.9	RHO	[29]

1. Introduction

Thermochemical Energy Storage (TES) uses the reversible chemical reactions and/or sorption processes of gases and vapours in solids or liquids. The principle is applicable in seasonal heat storage, as well as in sorption driven heat pumps, adsorption based cooling, *etc*. and the heat applied can be renewable, like sun heat, or waste heat [1]. One major benefit of using this method is that it only shows an insignificant amount of heat loss while reaching high energy storage densities [2]. At present, studies examine traditional (*e.g.* zeolites) and innovative (*e.g.* MOFs, aluminophosphates, porous carbons and composites) sorbents as sorption-based thermal energy storage materials [3–7].

As they have the potential for many application (gas capture/storage, catalysis, sensing, *etc.*), there has been an increased interest in metal-organic frameworks (MOFs) [8,9]. MOFs are a crystalline porous materials which are coordinated polymers formed from metal ion or clusters bridged by organic ligands [8,10]. One subgroup of MOFs is zeolitic imidazolate frameworks (ZIFs) [8]. ZIFs are comprised of transition metal ions (Zn, Co, *etc.*) and imidazolate linkers. The ZIF structure is connected in a similar manner as zeolites, where the metal ion and imidazolate linker replace the Si/Al and O atoms, respectively. ZIFs are considered to be highly stable. Due to their properties, including ordered porous structures and possibility to shape them in glass-like monoliths, ZIFs also have been proposed as supports for adsorptive separation applications [11]. Depending on the nature of functional groups on imidazolate ligands, ZIFs can be considered hydrophobic or hydrophilic.

In the last decade there has been increasing interest in examining the influence of various adsorbates in adsorption-driven applications for zeolites, aluminophosphates, COFs and MOFs, mainly focusing on water and short chain alcohols [12–21]. However, the reports on the optimization of ZIF for heat transformation applications are scarce and majority focusing on water as a working fluid. On the other hand, using ethanol instead of water in MOF-based systems is reportedly advantageous, which can be seen in a study by De Lange *et al.* (2015) [13]. They studied 18 different MOFs, among them one ZIF material, *i.e.* ZIF-8, for adsorption-driven heat pumps using methanol and ethanol. The study concluded that there are many benefits to using ethanol as a working fluid which include adsorption occurring at more applicable lower relative pressure [13]. Other studies which have been completed since have also highlighted the mechanisms of alcohol sorption in MOFs and ZIFs [6,20–23]. Our previous study completed in 2021, showed the preliminary study of hydrophobic ZIF-8 and hydrophilic ZIF-90 with water, ethanol and methanol as the working fluids. Prior to this study it was noted that no publications had employed differential scanning calorimetry (DSC) as rapid method to evaluate the heat storage potential of these materials. While the ZIF-90-water pairing proved to have the overall best performance, ZIF-8 had a higher affinity for ethanol adsorption. In a more recent study, Madero-Castro et al. (2024) examined the adsorption properties of hydrophobic ZIF-8, ZIF-71, ZIF-90, MAF-6 and MIL-140C while using methanol and ethanol as working fluids based on the processing of previously published adsorption data combined with a thermodynamic model [6]. The study show that the selected MOF-methanol pairings had the highest uptakes. It is worth noting, that while the study shows the ethanol uptake is lower, the adsorption occurs at lower pressures.

Based on the above, the goal of this study is to examine a wider range of ZIF structures for heat storage and allocation applications with water or ethanol as working fluids. The two main criteria for the materials selection was the pore entrance size and the pore/cage capacity of a particular ZIF. It is worth noting that reported data for these criteria are based on static measurements and subject to possible variations due to synthesis conditions, activation method, sorption-driven flexibility, *etc*. Five ZIFs with large pore entrance size and pore capacities, determined by the type of topology and presence of more or less bulky linker functional groups, were selected (Table 1) [24,30]. Additionally, two ZIFs with small pore entrance size and pore capacities were studied for comparison purposes (ZIF-62 and ZIF-74) [24,26]. Finally, our preliminary study on water, methanol and ethanol adsorption in ZIF-8 and ZIF-90 revealed that, although the same topology, different functional groups in both materials significantly affect the overall uptakes, with the most pronounced differences for water as adsorbate. Therefore, two ZIFs with hydrophilic functional groups and seven ZIFs with hydrophobic groups were selected (see Fig. 1). This study examines further the influence of morphology on the final uptakes as well as the stability of ZIFs after sorption experiments and estimates the adsorption enthalpies based on DSC data. Our results importantly expand the range of ZIFs for which data on the mechanism and thermodynamics of water and ethanol adsorption under the same experimental conditions is available.

2. Experimental

2.1. Materials

The materials and methods used for the synthesizing all ZIF samples are described in detail in the Supporting Information.

ZIF-8 was synthesised using the method from our previous study and used a 0.25: 1.25: 0.68 M ratio for zinc nitrate hexahydrate, 2-methylimidazole and N, N-dimethylformamide [21]. ZIF-62 was synthesised by modifying the Gustafsson & Zou (2013) method [31]. A 1:13:2:150 M

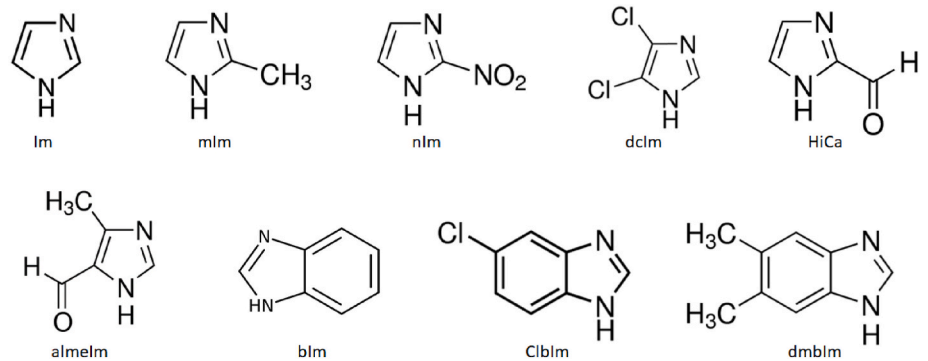

Fig. 1. Linkers for ZIF-8 (mIm), ZIF-62 (Im and bIm), ZIF-71 (dcIm), ZIF-74 (nIm and dmbIm), ZIF-76 (ClIm and Im), ZIF-90 (HiCa) and ZIF-93 (almeIm).

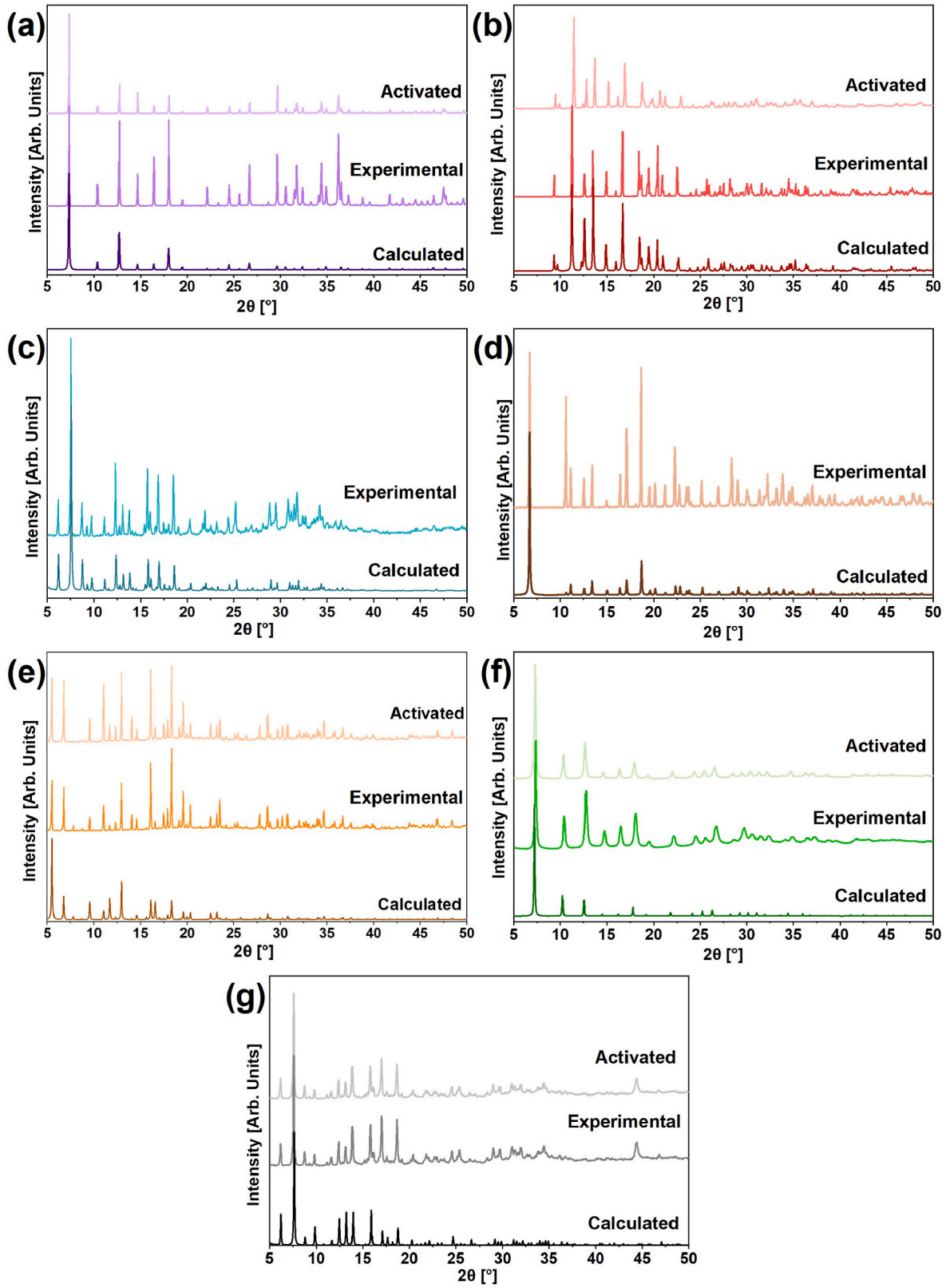

Fig. 2. Diffractograms showing calculated, experimental and activated PXRD patterns for (a) ZIF-8*, (b) ZIF-62, (c) ZIF-71, (d) ZIF-74, (e) ZIF-76, (f) ZIF-90* and (g) ZIF-93. *Notes results published from our previous study in Byrne et al. (2021), *Crystals,* 11, 1422.

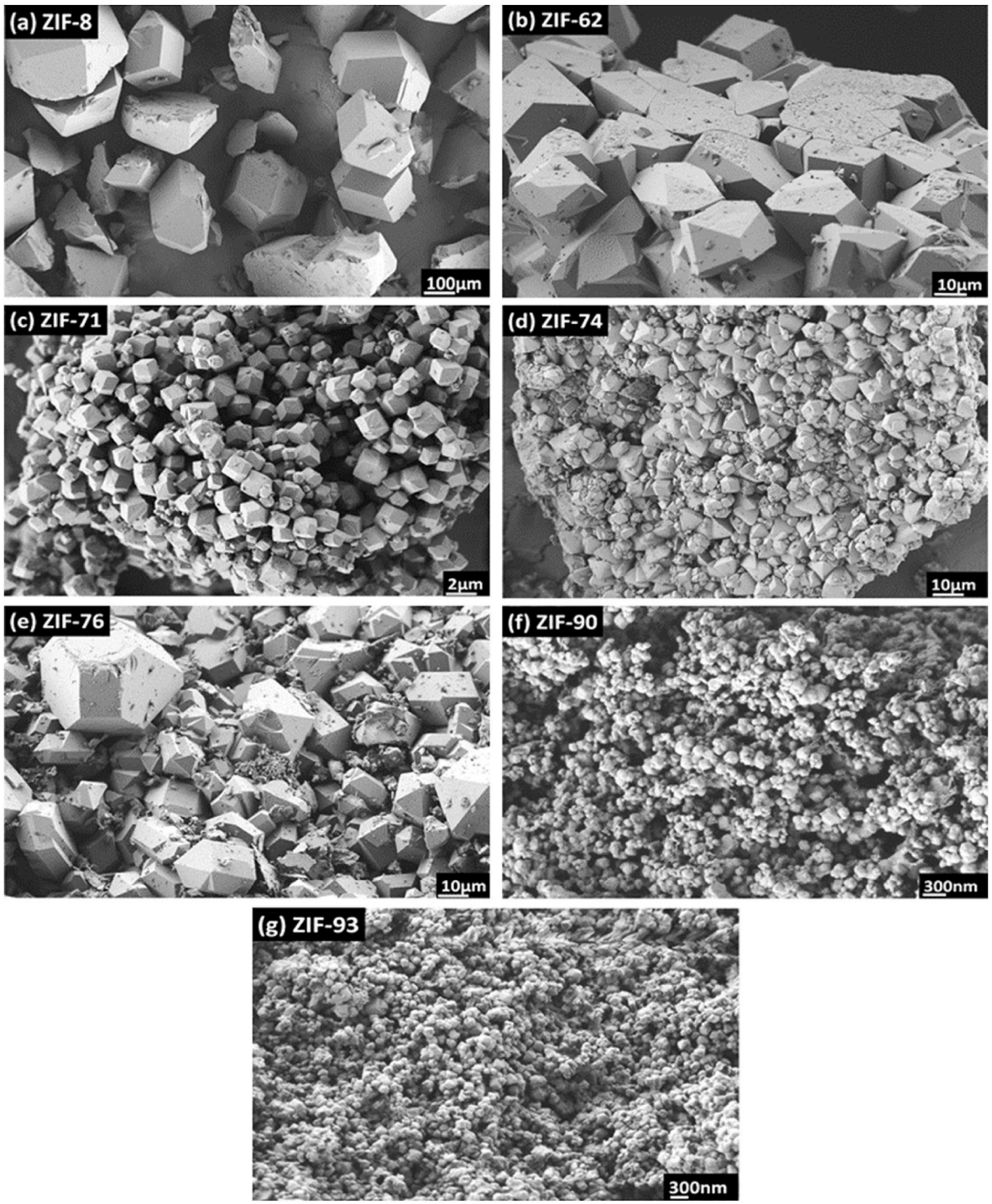

Fig. 3. SEM images of (a) ZIF-8, (b) ZIF-62, (c) ZIF-71, (d) ZIF-74, (e) ZIF-76, (f) ZIF-90 and (g) ZIF-93.

ratio for zinc nitrate hexahydrate, imidazole, benzimidazole and N, N-dimethylformamide for the synthesis of ZIF-62. ZIF-71 was prepared by modifying the Morris et al. (2010) method [29]. This synthesis used 0.66 mmol: 3.14 mmol: 1.48 mol for zinc nitrate hexahydrate, dichloroimidazole and methanol respectively. ZIF-74 was prepared based on the modification of the Banerjee et al. (2008) method [26]. A molar ratio of 1:2:2:150 was used for zinc nitrate hexahydrate, 2-Nitroimidazole, 5, 6-dimethylbenzimidazole and N, N-dimethylformamide respectively. ZIF-90 was synthesised based on the method published by Brown et al. (2012) [10]. The reaction ratio for zinc acetate dihydrate, 2-Imidazolecarboxaldehyde, N, N-dimethylformamide and methanol was 5 mmol: 20 mmol: 645 mmol: 1.23 mol respectively. ZIF-93 was synthesised using the procedure published by Gao et al. (2018) [30]. The synthesis of ZIF-93 used a 1:3:371 M ratio for zinc acetate dihydrate, 4-methyl-5-imidazolecarboxaldehyde and methanol.

2.2. Characterization

All samples were analysed with powder X-ray Diffraction (PXRD). The PXRD patterns were produced using a PANalytical X'Pert PRO diffractometer, using Cu Kα radiation (λ = 1.5418 Å). The diffraction range examined was between $2\theta = 5°–55°$ with a step size of 0.034° per

100 s using a fully opened 100 channel X'Celerator detector Plus.

The thermal stability of each ZIF sample was determined by completing thermogravimetric analysis (TGA) with a TA Instruments Q5000. The analysis performed in airflow (25 ml/min) and was heated from 25 to 800 °C at a ramp rate of 10 °C/min. TGA was repeated in the temperature range of 25–300 °C to determine the % of each adsorbate adsorbed.

The N_2 sorption isotherms were acquired at −196 °C on Quantachrome AUTOSORB iQ3. Before the adsorption analysis, the samples were degassed under vacuum at 150 °C for 10h. Brunauer–Emmett–Teller (BET) specific surface area was calculated from adsorption data in the relative pressure range from 0.005 to 0.02. The total pore volume (V_{total}) was calculated from the amount of N_2 adsorbed at $P/Po = 0.97$ and micropore volume (V_{micro}) from t-plot ($P/P_0 = 0.15–0.3$).

Scanning electron microscope (SEM) images were taken using a Zeiss Supra 35 VP microscope with an electron high tension voltage of 1.00 kV and Aperture Size 30.00 μm.

The $^{1}H–^{13}C$ CPMAS spectrum of the activated ZIF-8 sample was recorded on a 600 MHz Varian NMR spectrometer equipped with a 3.2 mm CPMAS probe. The sample was spun at 20 kHz, and 3200 scans were accumulated with a repetition delay of 2 s. A ^{1}H 90° pulse of 2.6 μs and a contact time of 5 ms were applied for cross-polarization, with high-power proton decoupling during acquisition. The ^{13}C MAS spectrum was acquired using a Hahn echo pulse sequence, with 90° and 180° pulses of 2.35 μs and 4.7 μs, respectively. A repetition delay of 120 s was used, and 20 scans were accumulated. The ^{13}C Larmor frequency was 150.71 MHz, and chemical shifts were referenced relative to tetramethylsilane (TMS).

2.3. Adsorption and desorption enthalpy studies

Ethanol and water sorption analysis was performed with an IGA-100 gravimetric analyzer (Hiden Isochema Ltd.). The samples were first degassed at 150 °C for 12 h to reach a constant weight. The isotherms were obtained at 25 °C in relative pressures of 0–0.9, where equilibrium was reached prior to moving onto the next step. Differential scanning calorimetry (DSC) was also carried out on all samples. Prior to DSC measurements, the ZIFs were placed in a desiccator containing water saturated solution of salt (NaCl, rh = 75 %) or ethanol for 1, 3 or 5 days. DSC analysis was completed on a Q2000 DSC apparatus (TA Instruments, Inc., USA) in the temperature range from 20 to 200 °C with the heating ramp of 5 °C/min. The desorption enthalpies were obtained the 'Integrate Peak linear' function that is a part of the TA Instruments Universal Analysis 2000 software.

3. Results & discussion

Seven different ZIF structures with varying topologies, pore entrances and pore capacities were synthesised by either using previously published methods or optimizing previously published methods. To confirm phase pure samples were produced and to analyse their structural and textural properties PXRD, TGA, N_2 physisorption and SEM were performed. In order to access their potential in heat storage applications, all samples were analysed using ethanol sorption and, for comparison water sorption studies as well as the DSC.

3.1. Structural properties

The crystalline structure and phase purity of all samples were determined using PXRD. This determination was completed by comparing the as-synthesised sample patterns to the calculated/simulated patterns based on their published structures (CIF files from structure database. CSD codes: ZIF-8 – VELVOY, ZIF-62 – GIZJOP, ZIF-71 - GITVIP01, ZIF-74 - GITVUB, ZIF-76 - GITWEM, ZIF-90 – WOJGEI and ZIF-93 - POVNEW). As it can be seen from Fig. 2, all ZIF samples proved to be phase pure with only slight deviations in the measured intensities.

Table 2
Nitrogen physisorption analysis for all ZIFs showing the specific surface area (S_{BET}), micro pore volume (V_{micro}) and total pore volume (V_{total}).

ZIF	S_{BET} [m^2/g]	V_{micro} [cm^3/g]	V_{total} [cm^3/g]
ZIF-8	621[a]	0.208	0.252[a]
ZIF-62	6	N/A[b]	N/A[b]
ZIF-71	1038	0.349	0.425
ZIF-74	N/A[b]	N/A[b]	N/A[b]
ZIF-76	972	0.331	0.411
ZIF-90	1119[a]	0.390	0.571[a]
ZIF-93	1058	0.255	0.393

[a] Notes results published from our previous study in Byrne et al. (2021), Crystals, 11, 1422.
[b] N/A indicates that it was not possible to obtain these readings for the relevant samples.

The PXRD patterns of the as-synthesised ZIFs were also used for the first estimation of the crystallite size using the Scherrer equation (Table S1). The calculations for ZIF-8 and ZIF-76 revealed the largest primary particle size of 400 nm. ZIF-90 exhibit the smallest crystallites of 20 nm. The sizes of the rest range from 90 to 180 nm.

TGA was then preformed on all the ZIFs to indicate if the samples required activation (*i.e.* removal of any solvent from the ZIF structure), see Fig. S1. This analysis showed that for ZIF-71 and ZIF-74 (Fig. S1 (c) & (d)), no activation was required while all the remaining ZIFs (ZIF-8, ZIF-62, ZIF-76, ZIF-90 & ZIF-93) needed activation. There are minor weight changes below 100 °C for ZIF-90 and ZIF-93 (Fig. S1 (f) & (g)), these are attributed to moisture on the surface of the powder samples and is a result of exposure to the atmosphere. PXRD confirmed that the ZIF structures remained intact after activation (see Fig. 2).

SEM analysis was used as an additional tool to check the particle size as well as the morphology and phase purity of the studied ZIFs. The images (Fig. 3) confirmed the phase purity of all prepared products, as indicated by the PXRD data and revealed characteristic morphologies of studied ZIFs [8,24–29]. However, there are significant differences in the degree of agglomeration of the primary particles among the samples. ZIF-8 (Fig. 3a) was seen in individual particles while the rest of ZIFs formed agglomerates. From SEM, the diameter of the ZIF-8 particles, as the largest ones, was estimated to be approx. 90 μm. For ZIF-90, the smallest ones, it was estimated to 150 nm in average. The trend in particle size mostly correlates with the trend noted by the calculated primary particle sizes from PXRD. However, the PXRD based estimates were smaller (i.e. 400 nm for ZIF-8 and 20 nm for ZIF-90) since Scherrer equation takes into account coherent scattering and exclude surface-related domains. Moreover, individual particles seen in the SEM images can be polycrystalline rather than single crystals ZIF-62 contain micron-sized particles. Calculation of their dimensions from Scherrer equation is therefore not valid in that case (Fig. 3 (b)). This variation might be due to a long synthesis time and static conditions of ZIF-62, where the crystal growth occurs at a slow rate and allows large agglomerates to form.

Nitrogen physisorption was completed to determine the specific surface area as well as the pore volume and pore size distribution of the ZIFs (see Fig. S2). The determined specific surface area for ZIF-62 was significantly lower than all of the other ZIFs, i.e. 6 m^2/g. Due to such low value, it was not possible to determine the micro or total pore volumes of ZIF-62. At the time of writing, it was not possible to find published data on the specific surface are of this ZIF using nitrogen as a probe molecule. This is expected due to small pore entrances that stop the nitrogen molecules to enter the pores and is in accordance with the literature [32]. Possibly for the same reason, it was not possible to obtain any readings from nitrogen physisorption for ZIF-74.

The specific surface area of all remaining ZIFs ranged from 621 to 1119 m^2/g. Among these, ZIF-8 has the smallest specific surface area, micro pore volume and total pore volume while ZIF-90 showed the highest results in all three parameters. As it can be seen in Table 2, the

Table 3
Ethanol sorption: relative pressure (P/P_0) at the 50 % uptake and uptake at 0.8 P/P_0 (mmol/g); Water sorption: at most common storage working pressure of 0.4 P/P_0 (mmol/g) and uptake at 0.8 P/P_0 (mmol/g).

ZIF	P/P_0 at 50 % EtOH uptake	Max EtOH uptake at 0.8 P/P_0 (mmol/g)	H_2O uptake at 0.4 P/P_0 (mmol/g)	Max H_2O uptake at 0.8 P/P_0 (mmol/g)
ZIF-8	0.07	4.7	1.1	3.4
ZIF-62	0.02	1.7	0.3	0.5[a]
ZIF-71	0.13	6.3	0.5	1.3
ZIF-74	–	0.1	–	–
ZIF-76	0.07	5.9	0.3	1.1
ZIF-90	0.13	4.9	12.9	17.8
ZIF-93	0.06	7.0	3.9	18.1[a]

[a] max H_2O uptake for ZIF-62 and ZIF93 was taken at 0.7 P/P0 and 0.75 P/P0 respectively.

share of mesoporosity is the largest for ZIF-90, which is due to the agglomeration of nanoparticles and associated introduction of inter-particle porosity, and the smallest for ZIF-8, *i.e.* the total pore volume for ZIF-8 is only 0.044 cm^3/g bigger than the micro pore volume, whereas for ZIF-90 it is 0.181 cm^3/g bigger [21,30,33]. As mentioned in our previous study, the specific surface area for ZIF-90 falls in the higher bracket of published data (394–1426 m^2/g) [21,30,33–37]. In contrast, ZIF-8 showed a significant reduction of the specific surface area (418–1801 m^2/g) [20,23,30,38–40]. Unusual low S_{BET} value of ZIF-8 and the large differences in specific surface area in the literature originate from various factors, including particle size and method of activation. In addition to generally reduced diffusivity, very large crystals (like in ZIF-8) can possess various structure imperfections (point defects, dislocations, stacking faults) also causing pore blockings and diffusion obstructions. Furthermore, trapped solvent DMF that is not completely removed during activation is another indication of occurrence of some 'dead end pockets' that results in reduced values. Indeed, NMR of the activated ZIF-8 used in our study revealed the presence of DMF in the sample (see Fig. S3). The two RHO ZIFs (ZIF-71 and ZIF-93) show a relatively similar specific surface area. Both of these values exceed results from previously published studies, with 604 m^2/g – 864 m^2/g for ZIF-93 and 652 m^2/g – 782 m^2/g for ZIF-71 [29,30,41–45]. Finally, the specific surface area of ZIF-76 is 972 m^2/g, which is less than 100 m^2/g smaller than ZIF-71 and ZIF-93 and is in the middle of range when compared with previously published work (526–1561 m^2/g) [46–49].

3.2. Sorption study

Previous reports on sorption studies for ZIFs have mainly focused on water uptake with ethanol sorption only gaining interest more recently [6]. How these results have been reported have varied, specifically the uptake (either in % or mmol/g) or what relative pressure the reading was taken at. In order to compare the results with some of the most relevant studies to ours, *e.g.* Ref. [13], we list for (1) ethanol the relative pressure (P/P_0) at the 50 % uptake, in addition to the uptake of the isotherm at 0.8 P/P_0, which was considered max uptake and for (2) water most commonly listed storage working pressure of 0.4 P/P_0 and the uptake of the isotherm at 0.8 P/P_0, which was considered max uptake (Table 3). To further make it easier to compare these results with previously published studies we have included all results in % uptake in the SI (see Tables S2 and S3).

Fig. 4 shows the ethanol and water isotherms for all examined materials. In addition, Fig. S4 shows the water and ethanol isotherms for ZIF-8 and ZIF-90 in comparative manner. First, it can clearly be seen that the hydrophobic ZIFs and small pore ZIFs practically do not adsorb water, while for ethanol adsorption the size of the pore is the only limitation. Additionally, Fig. 4, S5 and S6 shows that the water isotherm for ZIF-90 and the ethanol isotherm for ZIF-93 both have condensation at the end of the isotherm which is why the max uptake for all ZIF samples was taken at 0.8 P/P_0.

Due to the small size of the pore entrance and capacity for ZIF-62 and ZIF-74, it was expected that the uptake for both ZIFs and both adsorbates would be low. This theory proved to be correct, which can be seen in Figs. 4 and 5 as well as in Tables 4, S2 and S3. ZIF-74 had the overall lowest uptake for both adsorbates compared to all of the other ZIFs examined in this study. It was not possible to obtain a reading for ZIF-74 when water was used as the working fluid while with ethanol the uptake was only 0.1 mmol/g at both 0.4 and 0.8 P/P_0. ZIF-62 showed a higher uptake in both water and ethanol (Figs. 4 and 5 and Table 3) despite having a lower pore/cage capacity compare to ZIF-74. These differences are likely are a result of the difference in the pore/cage entrance and the different functional groups in the ZIFs. Additionally, the SEM images in Fig. 3 show that ZIF-74 agglomerates are more densely packed than those in ZIF-62 which results in hindering the access of the water/ethanol molecules to some of the pores. The previous studies on these two ZIFs have focused on synthesis methods, structural properties and theoretical analysis, however ZIF-62 has been extensively studied for formation of glasses [8,9,26,31,50,51].

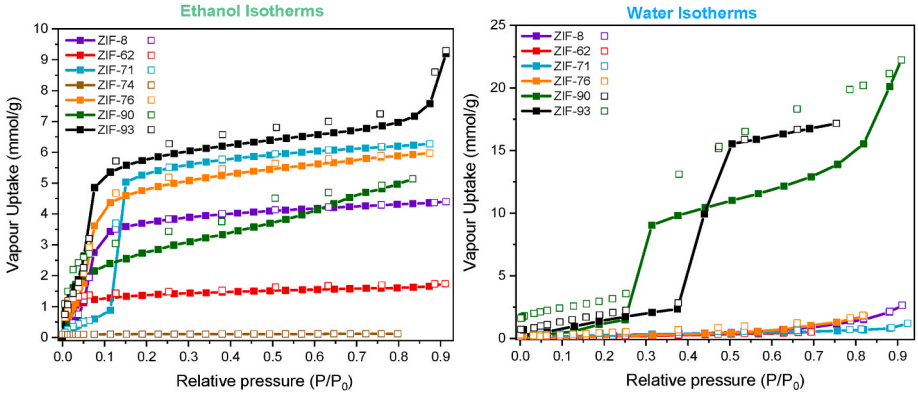

Fig. 4. Ethanol (left) and water (right) isotherms for ZIF samples studied which were obtained at 25 °C. The solid squares and lines represent the adsorption while the empty squares show the desorption of the working fluid. No water isotherm was obtained for ZIF-74.

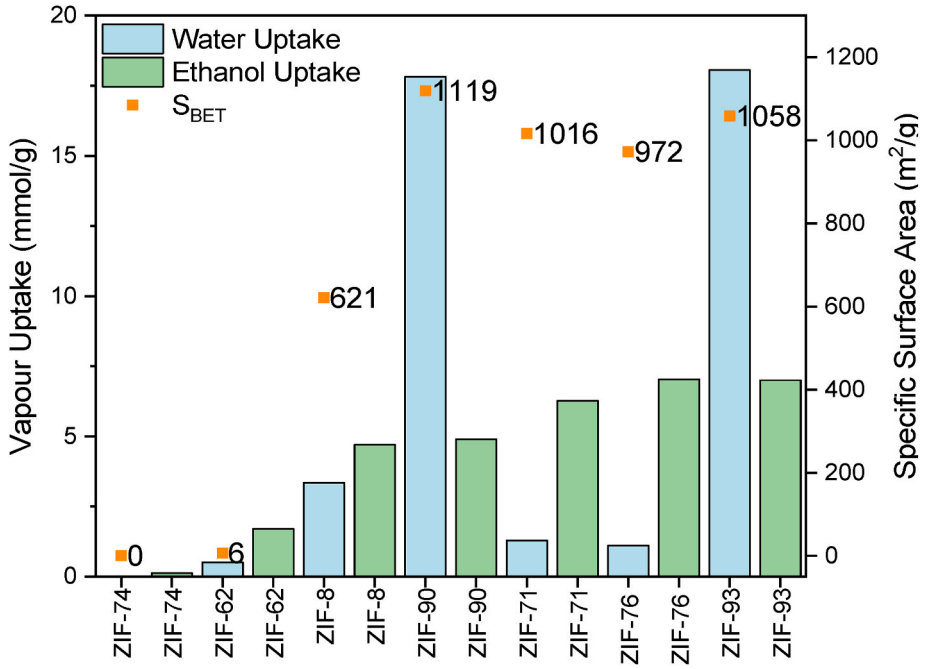

Fig. 5. Bar chart showing the ethanol and water uptake (mmol/g) obtained at 25 °C for all ZIFs at 0.8 P/P_0 as well as the specific surface area (S_{BET}) for all samples. The water uptake for ZIF-62 and ZIF-93 was take between 0.7 and 0.75 P/P_0.

The ethanol uptake for all six absorbing ZIFs (ZIF-8, ZIF-62, ZIF-71, ZIF-76, ZIF-90 and ZIF-93) is mostly completed below 0.2 P/P_0. The isotherms exhibit S-shapes (Type I, IV or Type V), except for ZIF-62 isotherm (Fig. 5 and Tables 4, S2 and S3). The ZIF-93 sample exhibits the highest ethanol uptake, followed by ZIF-71 and ZIF-76. The position of the isotherm inflection point for the three listed ZIFs is the lowest for ZIF-93 (0.06 P/P_0), followed by ZIF-76 (0.07 P/P_0) and for ZIF-71 (0.13 P/P_0).

On the other hand, the water, which is noteworthy adsorbed only in two ZIFs (ZIF-90, with only hydrophilic functional group, and ZIF-93, with hydrophilic and hydrophobic functional group) is adsorbed at relative pressures above 0.25 P/P_0, with only a slight incline after this (Fig. 4 and S4). The water isotherms exhibit S-shapes (Type V). The water uptakes at both 0.4 P/P_0 and 0.8 P/P_0 is very low for the three hydrophobic ZIFs.

The largest differences between water and ethanol uptake is seen for ZIF-71 and ZIF-76 structures. The max ethanol uptakes is ~5 times higher for ZIF-76 and ZIF-71. In contrast, ZIF-8 only showed a doubled uptake for ethanol than water.

In terms of the two hydrophilic ZIFs that were examined, ZIF-90 and ZIF-93 have a very similar max water uptake (Fig. 5). However, there is a vastly noticeable difference when the water uptake is taken at the working relative pressure 0.4 P/P_0 (Table 3 and Fig. S6). ZIF-90 has an uptake of 12.9 mmol/g at 0.4 P/P_0, which is 3.3 higher than the uptake of ZIF-93. This difference is due to the shift of inflection point of water isotherm towards higher relative pressures. As it can be seen in Fig. S6, the inflection for ZIF-90 occurs between 0.2 and 0.3 P/P_0 while the inflection for the ZIF-93 isotherm occurs between 0.35 and 0.5 P/P_0. This difference in inflection point for the two ZIFs is in line with previously published isotherms and with the presence of hydrophobic methyl group in ZIF-93 that induces the move towards higher relative pressures [30]. Furthermore, Fig. 5, which compares the water vapour uptake to the specific surface area, indicates that there is definitely not a direct correlation between the specific surface area and the water vapour loading in the ZIF structures. ZIF-8 and ZIF-90 share the same topology and pore entrance, with very similar pore and cage capacities. Despite ZIF-90 having an S_{BET} approximately 1.8 times greater than ZIF-8, the water uptake of ZIF-90 is five times higher than that of ZIF-8. We can conclude, that for water uptake the presence of hydrophilic group, *i.e.* a "hand" for first water molecules adsorption, in ZIF material is crucial and which directs the mechanism and the final water vapour uptake.

Table 4
Range of water and ethanol uptakes at max pressure (0.8 P/P_0) from previously published papers.

ZIF	Max EtOH uptake (mmol/g)	Ref.	Max H_2O uptake (mmol/g)	Ref.
ZIF-8	~5–6.5	[6,52,54]	0–2	[20,23,30,52,54–57]
ZIF-62	N/A	N/A	N/A	N/A
ZIF-71	~3.5–6	[6,52]	0–0.2	[20,52,58]
ZIF-74	N/A	N/A	N/A	N/A
ZIF-76	N/A	N/A	~0.4–2.5	[47]
ZIF-90	~6	[6]	~18–~22	[20,30,58]
ZIF-93	N/A	N/A	~20	[30]

N/A indicate that no previous data is available.

On the other hand, the ethanol uptake for the ZIF-8 and ZIF-90 differs by only ~0.7 mmol/g. Furthermore, ZIF-90, with the highest S_{BET} among the samples (1119 m^2/g) shows slightly lower ethanol uptake compared to ZIF-71, ZIF-76, and ZIF-93. These observations indicate that hydrophilicity could influence the final ethanol uptake, but to a much lesser extent than for water uptake, *i.e.* for the ethanol uptake, we could confirm the determining influence of the pore entrance/capacity on the final uptake, however, the position of the isotherm inflection point is influenced by the presence of hydrophilic functional groups.

The raw data for all isotherms is included in the SI (Tables S4–10).

As previously mentioned in the Introduction, there has been growing interest in the study of ZIFs with water and/or ethanol as working fluids for many applications [6,13,20,22,23,30,52,53]. Table 4 shows the previous reported water and ethanol uptakes for the ZIFs examined in this study.

Table 5
Desorption enthalpy (J/g) for all samples after soaking for 1 day, 3 days and 5 days.

ZIF	1 day		3 days		5 days	
	EtOH	H_2O	EtOH	H_2O	EtOH	H_2O
ZIF-8[a]	117.5	61.9	201.8	52.8	233.3	53.2
ZIF-62	30.7	–	35.7	–	41.9	–
ZIF-71	136.9	–	148.1	–	142.9	–
ZIF-74	–	–	–	–	–	–
ZIF-76	210.7	–	144.4	–	165.3	–
ZIF-90[a]	291.6	544.3	268.4	304.0	224.0	255.1
ZIF-93	289.8	503.5	293.9	488.4	306.6	503.7
Zeolite 13X	13.8	90.9	N/A	N/A	104.1	91.0

[a] Notes results published from our previous study in Byrne et al. (2021), Crystals, 11, 1422.

It is important to note that there are many factors which have caused variation in previously published sorption results as well as in this study, ranging from synthesis methods, the use of commercially available samples, difference in size of particles, variation in the specific surface area to the acquisition temperature of the isotherms. In general, smaller particles have a higher surface-to-volume ratio and can possess significant amount of terminal surface features such as hydroxyl groups, which can have a significant impact on adsorption capacities for water or/and ethanol by enhancing hydrophilicity and promote water adsorption over ethanol. Furthermore, disordered pore narrowing due to DMF remains can hinder diffusion of larger molecule (ethanol) in comparison to water and also cause a rise of hydrophilic character of the material.

For example in 2013, Zhang et al. examined ZIF-8, ZIF-71 and ZIF-90 for the adsorption of short chain alcohols and water for separation applications [20]. They showed that the max ethanol uptake for all three ZIFs is approx. 6 mmol/g, this is slightly lower than the ZIF-71 uptake in this study (Table 3) but 1.3 and 1.1 mmol/g higher that the ZIF-8 and ZIF-90 in Table 3 respectively. In the same study, it was found that the max water uptake for ZIF-8, ZIF-71 and ZIF-90 was ~0.3, ~0.2 and ~18 mmol/g respectively [20]. As it can be seen in Table 3, ZIF-8 and ZIF-71 show higher uptakes than this while there is only a difference of 0.2 mmol/g in the water uptake of ZIF-90. Probable reasons for the listed differences with our results are different synthesis methods for ZIF-71 and ZIF-90, the use of commercial ZIF-8, different activation methods and the sorption isotherms in the previous study were obtained at a higher temperature (308K/35 °C). It is possible that the presence of the DMF is what's caused the decrease in the S_{BET} as well as the increase in the water adsorption in our study.

3.3. DSC study

DSC has been previously used to study ZIFs heat storage potential, most of which focuses on water as a working fluid [21,59]. To date, only our previous study has performed DSC were alcohols as working fluids and this study only examines ZIF-8 and ZIF-90 [21]. Our approach, in which DSC is performed on samples exposed to selected adsorbates for varying durations, can be considered a simple screening method for preliminary estimations of adsorption kinetics and energetics. As it can be seen in that study and in Table 5, ZIF-90 showed higher desorption enthalpies for water for all 3 time points when compared to ethanol. For both working fluids, the longer the sample was in the desiccator the lower the desorption enthalpy. In contrast, ZIF-8 showed a clear preference to ethanol when compared with water and the desorption enthalpies increased the longer they were left in the ethanol desiccator [21]. There was only a change of 9.1 J/g for the water desorption enthalpies (Table 5). ZIF-90 showed the best overall result after being in the water desiccator for 1 day (544.3 J/g) [21]. These results indicate slower adsorption of larger ethanol molecule, if compared to water.

The desorption enthalpy of ZIF-93 was of great interest after it showed a very similar maximum water uptake to ZIF-90. Both of these ZIFs show their best overall result after being in the water desiccator for just one day, though ZIF-93's desorption enthalpy is 40.8 J/g lower than ZIF-90 (Table 5).What is of interest is that unlike ZIF-90, who's water desorption enthalpies reduce the longer it is in the desiccator, ZIF-93 remains considerably more stable. ZIF-90 desorption enthalpy reduces by 289.2 J/g by the 5th day in the desiccator while ZIF-93 shows a reduction after 3 days (down to 488.4 J/g) and then back to the starting value after 5 days (see Table 5 and Fig. 6).

The DSC results further confirmed the hydrophobic nature of ZIF-71 and ZIF-76 as it was not possible to get a reading for the two ZIFs for any of the day when soaked in water. As it can be seen in Fig. 7 (a) and (b), there are no distinct desorption peaks in graphs which made it impossible to determine the desorption enthalpy. As with the sorption studies, both ZIFs performed better than ZIF-8 with ethanol as the working fluid, particularly after 1 day in the desiccator containing ethanol. The desorption enthalpies for ZIF-71 and ZIF-76 after 1 day in the ethanol desiccator was ~1.2 and ~1.8 times higher than that of ZIF-8 (Fig. 7 (c)). In addition to these two ZIFs, ZIF-62 and ZIF-74 also showed no distinct peaks in the DSC (Fig. 7 (d) and (e)) and therefore it was not possible to determine their desorption enthalpies. This is unsurprising given the negligible water uptake for ZIF-62 and ZIF-74 during the sorption studies. ZIF-74 also showed no desorption enthalpy for any of the time points when ethanol was used as a working fluid, there were also no distinct peaks for these samples (see Fig. 7 (f)). Finally, while ZIF-62 does not have any clear peaks for any of the ethanol desorption enthalpies, the data for the three time points show a slight curvature in each of the lines (see Fig. 7 (g)), which made it possible to determine the desorption enthalpy (Table 5). However, it is worth evaluating if the data can be considered reliable due to the lack of clear peaks. This is where the ZIF-62 with ethanol and ZIF-8 with water samples differ as ZIF-8 has clear peaks, an example of this can be seen in Fig. 7 (g).

All samples (except ZIF74) were sent for PXRD after being placed in either desiccator for 5 days to determine if their structure remained stable. As mentioned in our previous study, ZIF-8 and ZIF-90 only had

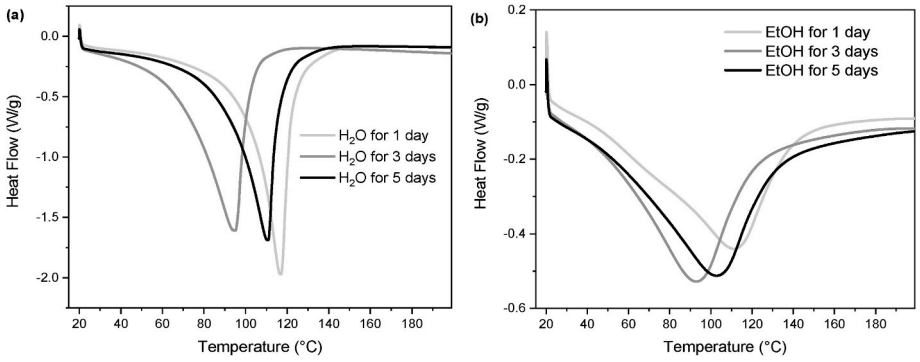

Fig. 6. DSC of ZIF-93 after 1, 3 and 5 days in the (a) water desiccator and (b) ethanol desiccator.

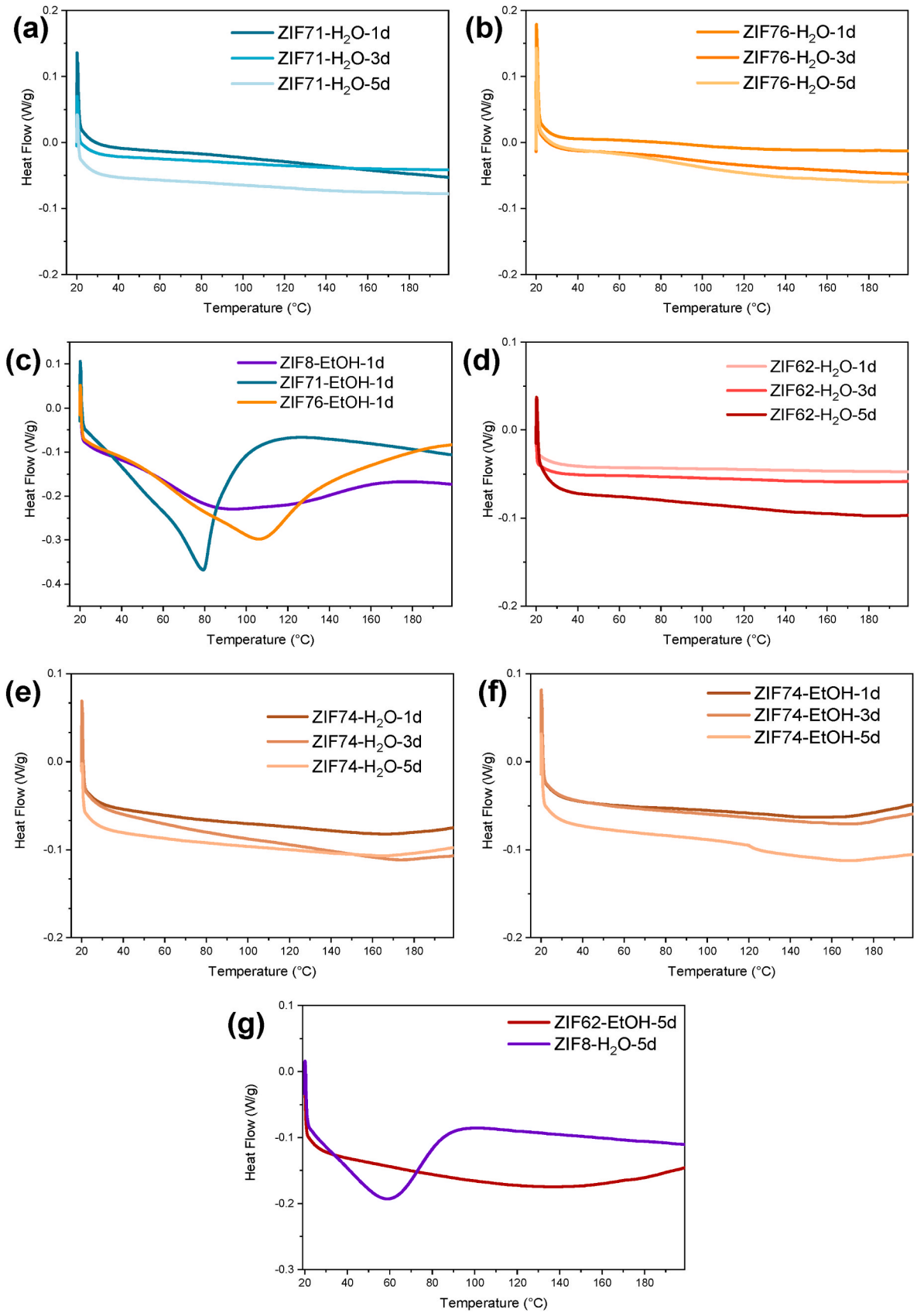

Fig. 7. DSC of (a) ZIF-71 with water as the working fluid, (b) ZIF-76 with water as the working fluid, (c) comparison of ZIF-8, ZIF-71 and ZIF-76 after 1 day in ethanol dissector, (d) ZIF-62 with water as the working fluid, (e) ZIF-74 with water as the working fluid, (f) ZIF-74 with ethanol as the working fluid and (g) comparison of ZIF-8 and ZIF-62 after 5 days in ethanol dissector.

minimal changes in the peak intensity when compared to the activated samples [21]. For the remaining ZIFs (ZIF-62, ZIF-71, ZIF-76 and ZIF-93), the structure remained intact though there were some variation in the peak intensities (see Fig. S7).

The desorption enthalpies for ZIF-93 and ZIF-90 only differ by approx. 3 J/g after 1 day in the ethanol desiccator, with ZIF-90 showing the higher result (see Table 5). In contrast to ZIF-90, there is a marginal increase (~17 J/g) in the desorption enthalpy for ZIF-93 when it is left in the ethanol desiccator for longer. ZIF-93 showed the best overall desorption enthalpy when ethanol is used as a working fluid.

In order to compare these results to that of the state-of-the-art, the results from the ZIF-90-water pairing after 1 day in the desiccator was used. As previously mentioned, the desorption enthalpy for this sample is 544.3 J/g (which is 151 Wh/kg). Despite an extensive literature review, it was only possible to find one other study that assessed ZIFs in a similar manner [21]. Once the search was expanded to all assessment methods, we found a study completed this year that ZIF-8, ZIF-71 and ZIF-90 when ethanol was used as the working fluid [6]. When compared to our study, the results from this publication are significantly lower for ZIF-8 (more than 3 times) and slightly lower for ZIF-90 (1.2 times) while for ZIF-71 it was ~1.5 times higher than this study. It is worth noting that Madero-Castro et al. found the best ZIF-working fluid pairing was ZIF-8 with methanol, which showed ~100 Wh/kg. One of the most studied MOFs in this area, MIL-160, has shown a significantly higher desorption enthalpies when compared to ZIFs, producing a result of 343 Wh/kg. Literature search indicated that the commercially available zeolite Y and zeolite 13X show similar heat storage potential as our best preforming ZIF (185 and 120 Wh/kg, respective) [3]. For comparison purposes, we completed a study on the commercially available Zeolite 13X using the exact same drying method as was used for the ZIFs and soaking in the desiccators for 1 and 5 days. As it can be seen in Table 5 and Fig. S8, the desorption enthalpies in this study when using water as a working fluid are substantially lower than those previously published results. The difference in the required drying/activation temperature between ZIFs and zeolites is likely the cause of the cause of the variation in results. At present, it was not possible to find any desorption enthalpies for zeolite 13X when ethanol was used as a working fluid. Finally, $AlPO_4$-LTA, which is generally considered the best preforming material in this area showed a result of 373 Wh/kg [7].

4. Conclusions

In this research, we examined seven ZIFs as adsorbents for adsorption based heat storage applications, using water and ethanol as working fluids. The results showed viable options for possible uses in TES applications. All ZIFs were synthesised using simplified methods and all cases proved to be phase pure samples. Uptake of ethanol/water can be effected by pore/cage entrance and capacity, functional groups of linkers, synthesis method and crystalline size. Our study showed that the functional group of the linkers has a significant impact on the water uptake. In contrast, these functional groups have little impact on the ethanol uptake. ZIF-93 had the highest max ethanol and water uptake, with ZIF-71 showing the next highest with ethanol (difference of 0.7 mmol/g) while ZIF-90 showed an uptake of 0.3 mmol/g lower when water was the working fluid. ZIF-90 had the highest desorption enthalpy with water as a working fluid, while ZIF-93 had the highest ethanol desorption enthalpy. However, ZIF-93 proved to be more stable for both working fluids. Therefore, it can be concluded that ZIF-93 has the greatest heat storage potential out of the seven ZIFs studied when examining both working fluids. This study sheds light on the interplay between ZIF structure and heat storage potential, paving the way for further exploration and optimization of ZIF-based materials in adsorptive separation and storage applications. Finally, this study clearly shows that main factor when selecting an adsorbent when ethanol is the working fluid is the pore size (i.e. capacity), while for water as the working fluid the criteria is the hydrophobicity of the linker/material.

CRediT authorship contribution statement

Ciara Byrne: Writing – original draft, Formal analysis, Conceptualization. **Matjaž Mazaj:** Writing – review & editing. **Nataša Zabukovec Logar:** Writing – review & editing, Funding acquisition.

Declaration of competing interest

The authors declare that they have no known competing financial interests or personal relationships that could have appeared to influence the work reported in this paper.

Acknowledgements

This research was funded by Slovenian Research Agency, Research program P1-0021.The authors would like to thank Mojca Opresnik for scanning electron microscope (SEM) imaging, Andraž Krajnc for Nuclear magnetic resonance (NMR) measurements and Edi Kranjc for powder X-ray Diffraction (PXRD).

Appendix A. Supplementary data

Supplementary data to this article can be found online at https://doi.org/10.1016/j.matchemphys.2024.130143.

Data availability

Data will be made available on request.

References

[1] S.K. Henninger, S.J. Ernst, L. Gordeeva, P. Bendix, D. Fröhlich, A.D. Grekova, L. Bonaccorsi, Y. Aristov, J. Jaenchen, New materials for adsorption heat transformation and storage, Renew. Energy 110 (2017) 59–68, https://doi.org/10.1016/j.renene.2016.08.041.

[2] H. Wu, F. Salles, J. Zajac, A critical review of solid materials for low-temperature thermochemical storage of solar energy based on solid-vapour adsorption in view of space heating uses, Molecules 24 (2019), https://doi.org/10.3390/molecules24050945.

[3] A. Ristić, F. Fischer, A. Hauer, N. Zabukovec Logar, Improved performance of binder-free zeolite y for low-temperature sorption heat storage, J. Mater. Chem. A. 6 (2018) 11521–11530, https://doi.org/10.1039/c8ta00827b.

[4] A. Ristić, N.Z. Logar, New composite water sorbents CaCl2-PHTS for low-temperature sorption heat storage: determination of structural properties, Nanomaterials 9 (2019), https://doi.org/10.3390/nano9010027.

[5] R.M. Madero-Castro, J.M. Vicent-Luna, X. Peng, S. Calero, Adsorption of linear alcohols in amorphous activated carbons: implications for energy storage applications, ACS Sustain. Chem. Eng. 10 (2022) 6509–6520, https://doi.org/10.1021/acssuschemeng.1c06315.

[6] R.M. Madero-Castro, A. Luna-Triguero, C. González-Galán, J.M. Vicent-Luna, S. Calero, Alcohol-based adsorption heat pumps using hydrophobic metal-organic frameworks, J. Mater. Chem. A. 12 (2023) 3434–3448, https://doi.org/10.1039/d3ta05258c.

[7] A. Krajnc, J. Varlec, M. Mazaj, A. Ristić, N.Z. Logar, G. Mali, Superior performance of microporous aluminophosphate with LTA topology in solar-energy storage and heat reallocation, Adv. Energy Mater. 7 (2017) 1–8, https://doi.org/10.1002/aenm.201601815.

[8] Y. Ban, Y. Peng, Y. Zhang, H. Jin, W. Jiao, A. Guo, P. Wang, Y. Li, W. Yang, Dual-ligand zeolitic imidazolate framework crystals and oriented films derived from metastable mono-ligand ZIF-108, Microporous Mesoporous Mater. 219 (2016) 190–198, https://doi.org/10.1016/j.micromeso.2015.08.013.

[9] Q. Xu, C. Zhong, A general approach for estimating framework charges in metal-organic frameworks, J. Phys. Chem. C 114 (2010) 5035–5042, https://doi.org/10.1021/jp910522h.

[10] A.J. Brown, J.R. Johnson, M.E. Lydon, W.J. Koros, C.W. Jones, S. Nair, Continuous polycrystalline zeolitic imidazolate framework-90 membranes on polymeric hollow fibers, Angew. Chemie - Int. Ed. 51 (2012) 10615–10618, https://doi.org/10.1002/anie.201206640.

[11] C. Zhou, L. Longley, A. Krajnc, G.J. Smales, A. Qiao, I. Erucar, C.M. Doherty, A. W. Thornton, A.J. Hill, C.W. Ashling, O.T. Qazvini, S.J. Lee, P.A. Chater, N. J. Terrill, A.J. Smith, Y. Yue, G. Mali, D.A. Keen, S.G. Telfer, T.D. Bennett, Metal-organic framework glasses with permanent accessible porosity, Nat. Commun. 9 (2018) 1–9, https://doi.org/10.1038/s41467-018-07532-z.

[12] M. Erdös, M.F. De Lange, F. Kapteijn, O.A. Moultos, T.J.H. Vlugt, In silico screening of metal-organic frameworks for adsorption-driven heat pumps and chillers, ACS Appl. Mater. Interfaces 10 (2018) 27074–27087, https://doi.org/10.1021/acsami.8b09343.

[13] M.F. De Lange, B.L. Van Velzen, C.P. Ottevanger, K.J.F.M. Verouden, L.C. Lin, T.J. H. Vlugt, J. Gascon, F. Kapteijn, Metal-organic frameworks in adsorption-driven heat pumps: the potential of alcohols as working fluids, Langmuir 31 (2015) 12783–12796, https://doi.org/10.1021/acs.langmuir.5b03272.
[14] M.F. De Lange, K.J.F.M. Verouden, T.J.H. Vlugt, J. Gascon, F. Kapteijn, Adsorption-driven heat pumps: the potential of metal-organic frameworks, Chem. Rev. 115 (2015) 12205–12250, https://doi.org/10.1021/acs.chemrev.5b00059.
[15] W. Li, X. Xia, S. Li, Screening of covalent-organic frameworks for adsorption heat pumps, ACS Appl. Mater. Interfaces 12 (2020) 3265–3273, https://doi.org/10.1021/acsami.9b20837.
[16] Y. Jiang, M.H. Bagheri, R.T. Loibl, S.N. Schiffres, Thermodynamic limits of adsorption heat pumps: a facile method of comparing adsorption pairs, Appl. Therm. Eng. 160 (2019) 113906, https://doi.org/10.1016/j.applthermaleng.2019.113906.
[17] M.H. Bagheri, S.N. Schiffres, Ideal adsorption isotherm behavior for cooling applications, Langmuir 34 (2018) 1908–1915, https://doi.org/10.1021/acs.langmuir.7b03989.
[18] F. Jeremias, D. Fröhlich, C. Janiak, S.K. Henninger, Water and methanol adsorption on MOFs for cycling heat transformation processes, New J. Chem. 38 (2014) 1846–1852, https://doi.org/10.1039/c3nj01556d.
[19] S. Kayal, S. Baichuan, B.B. Saha, Adsorption characteristics of AQSOA zeolites and water for adsorption chillers, Int. J. Heat Mass Transf. 92 (2016) 1120–1127, https://doi.org/10.1016/j.ijheatmasstransfer.2015.09.060.
[20] K. Zhang, R.P. Lively, M.E. Dose, A.J. Brown, C. Zhang, J. Chung, S. Nair, W. J. Koros, R.R. Chance, Alcohol and water adsorption in zeolitic imidazolate frameworks, Chem. Commun. 49 (2013) 3245–3247, https://doi.org/10.1039/c3cc39116g.
[21] C. Byrne, A. Risti, S. Mal, M. Opresnik, N. Zabukovec Logar, A. Ristić, S. Mal, M. Opresnik, N.Z. Logar, A. Risti, S. Mal, M. Opresnik, N. Zabukovec Logar, A. Ristić, S. Mal, M. Opresnik, N.Z. Logar, Evaluation of ZIF-8 and ZIF-90 as heat storage materials by using water, methanol and ethanol as working fluids, Crystals 11 (2021) 1422, https://doi.org/10.3390/cryst11111422.
[22] Y. Du, K. Mao, B. Wooler, A.K. Sharma, D. Colmyer, M. Nines, S.C. Weston, Insights into the flexibility of ZIF-7 and its structural impact in alcohol adsorption, J. Phys. Chem. C 121 (2017) 28090–28095, https://doi.org/10.1021/acs.jpcc.7b10339.
[23] E. Hunter-Sellars, P.A. Saenz-Cavazos, A.R. Houghton, S.R. McIntyre, I.P. Parkin, D.R. Williams, Sol–gel synthesis of high-density zeolitic imidazolate framework monoliths via ligand assisted methods: exceptional porosity, hydrophobicity, and applications in vapor adsorption, Adv. Funct. Mater. 31 (2021) 12–14, https://doi.org/10.1002/adfm.202008357.
[24] A. Phan, C.J. Doonan, F.J. Uribe-romo, C.B. Knobler, M.O. Keeffe, O.M. Yaghi, Capture properties of zeolitic imidazolate frameworks, Acc. Chem. Res. 43 (2010) 58–67. http://www.ncbi.nlm.nih.gov/pubmed/19877580.
[25] X. Huang, J. Zhang, X. Chen, [Zn(bim)2] · (H2O)1.67: a metal-organic open-framework with sodalite topology, Chinese Sci. Bull. 48 (2003) 1531–1534, https://doi.org/10.1007/bf03183954.
[26] R. Banerjee, A. Phan, B. Wang, C. Knobler, H. Furukawa, M. O'Keeffe, O.M. Yaghi, High-throughput synthesis of zeolitic imidazolate frameworks and application to CO2 capture, Science 319 (2008) 939–943, https://doi.org/10.1126/science.1152516.
[27] D. Peralta, G. Chaplais, A. Simon-Masseron, K. Barthelet, C. Chizallet, A. A. Quoineaud, G.D. Pirngruber, Comparison of the behavior of metal-organic frameworks and zeolites for hydrocarbon separations, J. Am. Chem. Soc. 134 (2012) 8115–8126, https://doi.org/10.1021/ja211864w.
[28] W. Morris, C.J. Doonan, H. Furukawa, R. Banerjee, O.M. Yaghi, Crystals as molecules: postsynthesis covalent functionalization of zeolitic imidazolate frameworks, J. Am. Chem. Soc. 130 (2008) 12626–12627, https://doi.org/10.1021/ja805222x.
[29] W. Morris, B. Leung, H. Furukawa, O.M.K. Yaghi, N. He, H. Hayashi, Y. Houndonougbo, M. Asta, B.B. Laird, O.M.K. Yaghi, A combined experimental-computational investigation of carbon dioxide capture in a series of isoreticular zeolitic imidazolate frameworks, J. Am. Chem. Soc. 132 (2010) 11006–11008, https://doi.org/10.1021/ja104035j.
[30] M. Gao, J. Wang, Z. Rong, Q. Shi, J. Dong, A combined experimental-computational investigation on water adsorption in various ZIFs with the SOD and RHO topologies, RSC Adv. 8 (2018) 39627–39634, https://doi.org/10.1039/c8ra08460b.
[31] M. Gustafsson, X. Zou, Crystal formation and size control of zeolitic imidazolate frameworks with mixed imidazolate linkers, J. Porous Mater. 20 (2013) 55–63, https://doi.org/10.1007/s10934-012-9574-1.
[32] R.N. Widmer, G.I. Lampronti, S. Anzellini, R. Gaillac, S. Farsang, C. Zhou, A. M. Belenguer, C.W. Wilson, H. Palmer, A.K. Kleppe, M.T. Wharmby, X. Yu, S. M. Cohen, S.G. Telfer, S.A.T. Redfern, F.X. Coudert, S.G. MacLeod, T.D. Bennett, Pressure promoted low-temperature melting of metal–organic frameworks, Nat. Mater. 18 (2019) 370–376, https://doi.org/10.1038/s41563-019-0317-4.
[33] A. Škrjanc, C. Byrne, N. Zabukovec Logar, Green solvents as an alternative to DMF in ZIF-90 synthesis, Molecules 26 (2021), https://doi.org/10.3390/molecules26061573.
[34] M. Ghahramaninezhad, F. Mohajer, M. Niknam Shahrak, Improved CO2 capture performances of ZIF-90 through sequential reduction and lithiation reactions to form a hard/hard structure, Front. Chem. Sci. Eng. 14 (2020) 425–435, https://doi.org/10.1007/s11705-019-1873-5.
[35] Q. Zhang, S. Luo, J. Weidman, R. Guo, Surface modification of ZIF-90 with triptycene for enhanced interfacial interaction in mixed-matrix membranes for gas separation, J. Polym. Sci. 58 (2020) 2675–2687, https://doi.org/10.1002/pol.20200123.
[36] F.K. Shieh, S.C. Wang, S.Y. Leo, K.C.W. Wu, Water-based synthesis of zeolitic imidazolate framework-90 (ZIF-90) with a controllable particle size, Chem. Eur J. 19 (2013) 11139–11142, https://doi.org/10.1002/chem.201301560.
[37] H. Zhang, C. Duan, F. Li, X. Yan, H. Xi, Green and rapid synthesis of hierarchical porous zeolitic imidazolate frameworks for enhanced CO2 capture, Inorganica Chim. Acta. 482 (2018) 358–363, https://doi.org/10.1016/j.ica.2018.06.034.
[38] J.A. Thompson, K.W. Chapman, W.J. Koros, C.W. Jones, S. Nair, Sonication-induced Ostwald ripening of ZIF-8 nanoparticles and formation of ZIF-8/polymer composite membranes, Microporous Mesoporous Mater. 158 (2012) 292–299, https://doi.org/10.1016/j.micromeso.2012.03.052.
[39] X. Xia, Z. Liu, S. Li, Adsorption characteristics and cooling/heating performance of COF-5, Appl. Therm. Eng. 176 (2020) 115442, https://doi.org/10.1016/j.applthermaleng.2020.115442.
[40] N.A.H.M. Nordin, A.F. Ismail, A. Mustafa, R.S. Murali, T. Matsuura, The impact of ZIF-8 particle size and heat treatment on CO2/CH4 separation using asymmetric mixed matrix membrane, RSC Adv. 4 (2014) 52530–52541, https://doi.org/10.1039/c4ra08460h.
[41] Y. Li, L.H. Wee, J.A. Martens, I.F.J. Vankelecom, ZIF-71 as a potential filler to prepare pervaporation membranes for bio-alcohol recovery, J. Mater. Chem. A. 2 (2014) 10034–10040, https://doi.org/10.1039/c4ta00316k.
[42] E.V. Ramos-Fernandez, A. Grau-Atienza, D. Farrusseng, S. Aguado, A water-based room temperature synthesis of ZIF-93 for CO2 adsorption, J. Mater. Chem. A. 6 (2018) 5598–5602, https://doi.org/10.1039/c7ta09807c.
[43] Y. Ding, H. Wang, M. Yu, W. Zheng, X. Ruan, X. Li, Y. Xi, Y. Dai, H. Liu, G. He, Amine group graft ZIF-93 to create gas storage space to improve the gas separation performance of Pebax-1657 MMMs, Sep. Purif. Technol. 309 (2023) 122949, https://doi.org/10.1016/j.seppur.2022.122949.
[44] S. Japip, H. Wang, Y. Xiao, T.S. Chung, Highly permeable zeolitic imidazolate framework (ZIF)-71 nano-particles enhanced polyimide membranes for gas separation, J. Memb. Sci. 467 (2014) 162–174, https://doi.org/10.1016/j.memsci.2014.05.025.
[45] J.M. Luque-Alled, L. Martínez-Izquierdo, P. Gorgojo, C. Téllez, J. Coronas, Organic solvent-free fabrication of thin film polyamide/zeolitic imidazolate framework membranes for removal of dyes from water, Chem. Eng. J. 470 (2023), https://doi.org/10.1016/j.cej.2023.144233.
[46] D. Peralta, G. Chaplais, A. Simon-Masseron, K. Barthelet, G.D. Pirngruber, Synthesis and adsorption properties of ZIF-76 isomorphs, Microporous Mesoporous Mater. 153 (2012) 1–7, https://doi.org/10.1016/j.micromeso.2011.12.009.
[47] M. Švegovec, A. Škrjanc, A. Krajnc, N.Z. Logar, Green synthesis approaches toward preparation of ZIF-76 and its thermal behavior, Cryst. Growth Des. 23 (2023) 3754–3760, https://doi.org/10.1021/acs.cgd.3c00137.
[48] T. Pham, K.A. Forrest, H. Furukawa, J. Eckert, B. Space, Hydrogen adsorption in a zeolitic imidazolate framework with lta topology, J. Phys. Chem. C 122 (2018) 15435–15445, https://doi.org/10.1021/acs.jpcc.8b04027.
[49] J. Pérez-Pellitero, H. Amrouche, F.R. Siperstein, G. Pirngruber, C. Nieto-Draghi, G. Chaplais, A. Simon-Masseron, D. Bazer-Bachi, D. Peralta, N. Bats, Adsorption of CO2, CH4, and N2 on zeolitic imidazolate frameworks: experiments and simulations, Chem. Eur J. 16 (2010) 1560–1571, https://doi.org/10.1002/chem.200902144.
[50] A.M. Bumstead, M.L. Ríos Gómez, M.F. Thorne, A.F. Sapnik, L. Longley, J. M. Tuffnell, D.S. Keeble, D.A. Keen, T.D. Bennett, Investigating the melting behaviour of polymorphic zeolitic imidazolate frameworks, CrystEngComm 22 (2020) 3627–3637, https://doi.org/10.1039/d0ce00408a.
[51] S. Li, R. Limbach, L. Longley, A.A. Shirzadi, J.C. Walmsley, D.N. Johnstone, P. A. Midgley, L. Wondraczek, T.D. Bennett, Mechanical properties and processing techniques of bulk metal-organic framework glasses, J. Am. Chem. Soc. 141 (2019) 1027–1034, https://doi.org/10.1021/jacs.8b11357.
[52] J. Wang, J. Wu, B. Zheng, J. Wang, Q. Shi, J. Dong, Adsorptive separation of butanol, acetone and ethanol in zeolite imidazolate frameworks with desirable pore apertures, Chem. Eng. Sci. 248 (2022) 117251, https://doi.org/10.1016/j.ces.2021.117251.
[53] H. Yin, P. Cay-Durgun, T. Lai, G. Zhu, K. Engebretson, R. Setiadji, M.D. Green, M. L. Lind, Effect of ZIF-71 ligand-exchange surface modification on biofuel recovery through pervaporation, Polymer (Guildf). 195 (2020) 122379, https://doi.org/10.1016/j.polymer.2020.122379.
[54] K. Zhang, R.P. Lively, C. Zhang, W.J. Koros, R.R. Chance, Investigating the intrinsic ethanol/water separation capability of ZIF-8: an adsorption and diffusion study, J. Phys. Chem. C 117 (2013) 7214–7225, https://doi.org/10.1021/jp401548b.
[55] A. Škrjanc, M. Opresnik, M. Gabrijelčič, A. Šuligoj, G. Mali, N. Zabukovec Logar, Impact of dye encapsulation in ZIF-8 on CO2, water, and wet CO2 sorption, Molecules 28 (2023) 1–11, https://doi.org/10.3390/molecules28207056.
[56] A.U. Ortiz, A.P. Freitas, A. Boutin, A.H. Fuchs, F.X. Coudert, What makes zeolitic imidazolate frameworks hydrophobic or hydrophilic? the impact of geometry and functionalization on water adsorption, Phys. Chem. Chem. Phys. 16 (2014) 9940–9949, https://doi.org/10.1039/c3cp54292k.
[57] K. Eum, K.C. Jayachandrababu, F. Rashidi, K. Zhang, J. Leisen, S. Graham, R. P. Lively, R.R. Chance, D.S. Sholl, C.W. Jones, S. Nair, Highly tunable molecular sieving and adsorption properties of mixed-linker zeolitic imidazolate frameworks, J. Am. Chem. Soc. 137 (2015) 4191–4197, https://doi.org/10.1021/jacs.5b00803.
[58] S. Calero, P. Gómez-Álvarez, Underlying adsorption mechanisms of water in hydrophobic and hydrophilic zeolite imidazolate frameworks: ZIF-71 and ZIF-90, J. Phys. Chem. C 119 (2015) 23774–23780, https://doi.org/10.1021/acs.jpcc.5b07360.
[59] Y. Luo, W. Cui, Y. Zou, H. Chu, F. Xu, L. Sun, Thermal decompositions and heat capacities study of a co-based zeolitic imidazolate framework, J. Therm. Anal. Calorim. 142 (2020) 891–898, https://doi.org/10.1007/s10973-020-09258-x.